Chapter 14

Intra-Left Ventricular Diastolic and Systolic Flow Velocity Distributions, based on Colour Doppler Echo Vector Flow Mapping of Normal Subjects and Heart Failure Patients

Thu-Thao Le, Dhanjoo Ghista, Ru-San Tan, and Sridhar Idapalapati

Prologue

The left ventricle (LV) is the biological pump for circulation, and the left atrium (LA) plays a major role in filling the LV in a way as to facilitate directed blood flow for ejection into the aorta by its contraction process. The LA transfers blood to LV in 2 steps: in the first step, the pressure gradient between LA and LV causes blood to passively flow into the LV at velocity E; the second step filling is caused by LA contraction, at filling velocity A. In a healthy heart, the E velocity is greater than the A velocity. The reduced value of the E/A ratio is often accepted as a clinical marker of diastolic dysfunction, in which the LV becomes so stiff as to impair proper filling, which can lead to diastolic heart failure

Intra-cardiac flow is useful for evaluating cardiac function, as it is the end-result of cardiac myocardial abnormalities. The vortex flow during left ventricular filling is a critical determinant of directed blood flow during ejection, and can offer a novel index of cardiac dysfunction. Vector flow mapping (VFM) technique has been recently developed to generate flow velocity vector fields by post-processing colour Doppler echo images. In this technique, axial velocity is measured from colour Doppler images, while radial velocity is computed by deconstructing the flow into a basic non-vortical laminar motion and a vortical component.

In normal subjects, after flow ejection into LV, the direction of flow is reversed towards the apex with a brief appearance of vortex at the early stage of isovolumic relaxation time. The major diastolic anterior vortex develops immediately after the onset of the early diastolic phase. This vortex continues during diastasis, persists into late LV filling phase and throughout isovolumic contraction phase and dissipates with the opening of the aortic valve and LV ejection. By using color-Doppler derived VFM, the intra-ventricular vortex flow can be determined for the detection of pathologically altered flow characteristics and identification of new pathophysiologic mechanisms in the development of cardiac disease.

We have carried out Clinical Studies to determine intra-LV flow patterns for HF patients (both HFNEF and HFREF) and normal subjects. Colour Doppler flow images were captured at the 3-chamber view for visualization of both inflow through mitral valve and outflow into the aorta. Intra-LV flow was determined using the VFM analysis package. In this technique, colour Doppler velocity (axial velocity, $\mathbf{u}$) profile was analysed across an arc at each echo depth. The measured Doppler velocity $\mathbf{u}$ along the beam line is composed of basic non-vortical laminar flow ($\mathbf{u_b}$) and vortex flow ($\mathbf{u_v}$) components. The basic flow component $\mathbf{u_b}$ is computed as $\mathbf{u_b}=\mathbf{u}-\mathbf{u_v}$. Then the vortex flow velocity components u_v (along the Doppler beam) and $\mathbf{v_v}$ (perpendicular to the Doppler beam) are obtained in terms of the stream function $\psi(r,\theta)$ as $\mathbf{u_v}=\frac{1}{r}\frac{\partial\psi}{\partial\theta}$ and $\mathbf{v_v}=-\frac{\partial\psi}{\partial\theta}$. The radial basic flow component $\mathbf{v_b}$ is obtained from $\mathbf{u_b}$ as $\mathbf{v_b}=\mathbf{u_b}tan\theta$. The flow velocity $\mathbf{U}(r,\theta)$ is then calculated as: $\mathbf{U}(r,\theta)=\big(\mathbf{u_b}(r,\theta)+\mathbf{u_v}(r,\theta)\big)\mathbf{i}(r,\theta)+\big(\mathbf{v_b}(r,\theta)+\mathbf{v_v}(r,\theta)\big)\mathbf{j}(r,\theta)$,

where (i) $\mathbf{i}(r,\theta)$ and $\mathbf{j}(r,\theta)$ are the unit vectors in the axial and radial direction, respectively, at point (r,θ); (ii) $\mathbf{u_b}$ and $\mathbf{u_v}$ are in the axial Doppler beam direction, while $\mathbf{v_b}$ and $\mathbf{v_v}$ are in the radial direction perpendicular to the Doppler beam.

The contractility index $d\sigma^*/dt_{max}$ is formulated as: $d\sigma^*/dt_{max} = 1.5 \times \frac{dV/dt_{max}}{MV}$, where dV/dt_{max} is the maximal flow rate into the aorta, measured at the LVOT using VFM, and MV is the myocardial volume, calculated as a quotient of LV mass (determined from M-mode images) and myocardial density (assumed to be 1.05g/ml).

We selected two groups of subjects for our clinical study: Group 1 consists of HFNEF1 and HFNEF2 and one normal subject1; Group 2 consists of HFREF1 and HFREF2 and one normal subject2.

In Diastolic Flow Patterns (illustrated in Fig 6), in the rapid filling phase, straight flow is seen to rush into the LV from the LA; circulating flow patterns are seen at the anterior and posterior walls of the LV in all subjects. In HFNEF patients there is no inflow during the diastasis phase, whereas in HFREF patients the flow continues to enter the LV with 2 circulating flow patterns seen at the anterior and posterior walls. The flow patterns for diastasis phase and atrial contraction phases are illustrated, and are marked by circulating flow patterns, prominently at the anterior wall, until the end of atrial contraction. Markedly prolonged diastasis phase is seen in both HFNEF patients.

In Systolic flow patterns (illustrated in Fig 8), it is seen that LV contraction produced recirculating flow patterns and directed flow towards the aortic valve. At early systole, flow is seen to be pouring out of the LV; however, recirculating flow is observed in all subjects. The flow gets ejected into the aorta rapidly at mid systole, and is gradually reduced at the end of systole (frame 4). In subjects HFNEF1, HFREF1 and HFREF2, the abnormal recirculating flow patterns, formed during isovolumic contraction, are seen to remain until the end of the systolic phase. Peak flow rate out of LV is reduced in HFREF patients.

The Results, as summarised in Table 2, show (i) substantially reduced values of contractility index for HFREF1 and HFREF2, (ii) low flow rates during atrial contraction in subjects HFREF1, HFNEF2, HFREF2 and Normal2, and (iii) marked reduction of peak systolic outflow rate in HFREF patients. We have been able to demonstrate the use of VFM technique to visualize blood flow patterns in HF patients and normal subjects, abnormal circulating flow patterns in filling, and irregularly directed flow patterns towards the aortic valve for HFREF patients. The VFM analysis has provided similar common flow patterns to those obtained from the combination of CFD and MRI, and contrast echo. This technique employs colour Doppler echo images which are routinely acquired in clinical settings, and thus, has great clinical potential.

1. Introduction: Mitral Velocities, Intra-Cardiac Flow, Heart Failure, Intra-LV Flow Patterns

1.1 Left Ventricular and Left Atrial Dynamics

The left ventricle (LV) is a biological pump for moving blood throughout the body. The left atrium (LA) is separated from the LV by the mitral valve. The LA transfers blood to LV in 2

steps: in the first step, the pressure gradient between LA and LV and the weight of the collected blood in LA causes blood to passively flow into the LV when the mitral valve opens. The speed at which the blood moves during this initial action is called the early or "E" filling velocity. Most filling (70-75%) of the ventricle occurs during this phase. But some blood always remains, so toward the end of the atrial emptying cycle (diastole), the second step occurs in which the LA contracts to squeeze out that last bit ("atrial kick"). The speed of the blood filling the ventricle in this step is the "A" (for atrial) filling velocity. Mitral E velocity reflects LA-LV pressure gradient during early diastole, which is affected by LA compliance and alterations in LV relaxation. Mitral A velocity reflects active filling of LV by LA contraction setting up LA-LV pressure gradient during late diastole.

The E/A ratio is the ratio of the early (E) to late (A) LV filling velocities. Pulsed-wave (PW) Doppler echocardiography (echo) allows the measurement of velocities at the level of the sample volume as seen in Figure 1. In a healthy heart, the E velocity is greater than the A velocity. In certain pathologies and with aging, the left ventricular wall can become stiff, increasing the back pressure as it fills, which slows the early (E) filling velocity, thus lowering the E/A ratio. The reduced value of the E/A ratio is often accepted as a clinical marker of diastolic dysfunction, in which the LV becomes so stiff as to impair proper filling, which can lead to diastolic heart failure. The deceleration time (DT) is the time taken from the maximum E point to baseline. DT is influenced by LV relaxation, LV diastolic pressure following mitral valve (MV) opening and LV compliance. Normally in adults it is less than 240ms.

The velocity of early myocardial relaxation as the mitral annulus ascends during early LV filling (E’), measured by tissue Doppler imaging (TDI), correlates well with invasive haemodynamic measures of time constant of isovolumic relaxation. In healthy young subjects, septal E’ is more than 10 cm/s and lateral more than 15 cm/s at rest. In patients with diastolic dysfunction related to a myocardial abnormality or disease, it is unusual that E’ velocity remains normal [1].

Based on E’ velocity and E/A ratio, a number of grades of diastolic function can be determined:

1. Normal diastolic function (E/A < 1),
2. Impaired relaxation (E/A reversal i.e. E/A > 1, DT>240ms, and reduced E’),
3. Pseudonormal (E/A ratio appears normal but E’ is reduced)
4. Restrictive filling (E/A ratio often >2 with a very short DT <160ms, reduced E’)

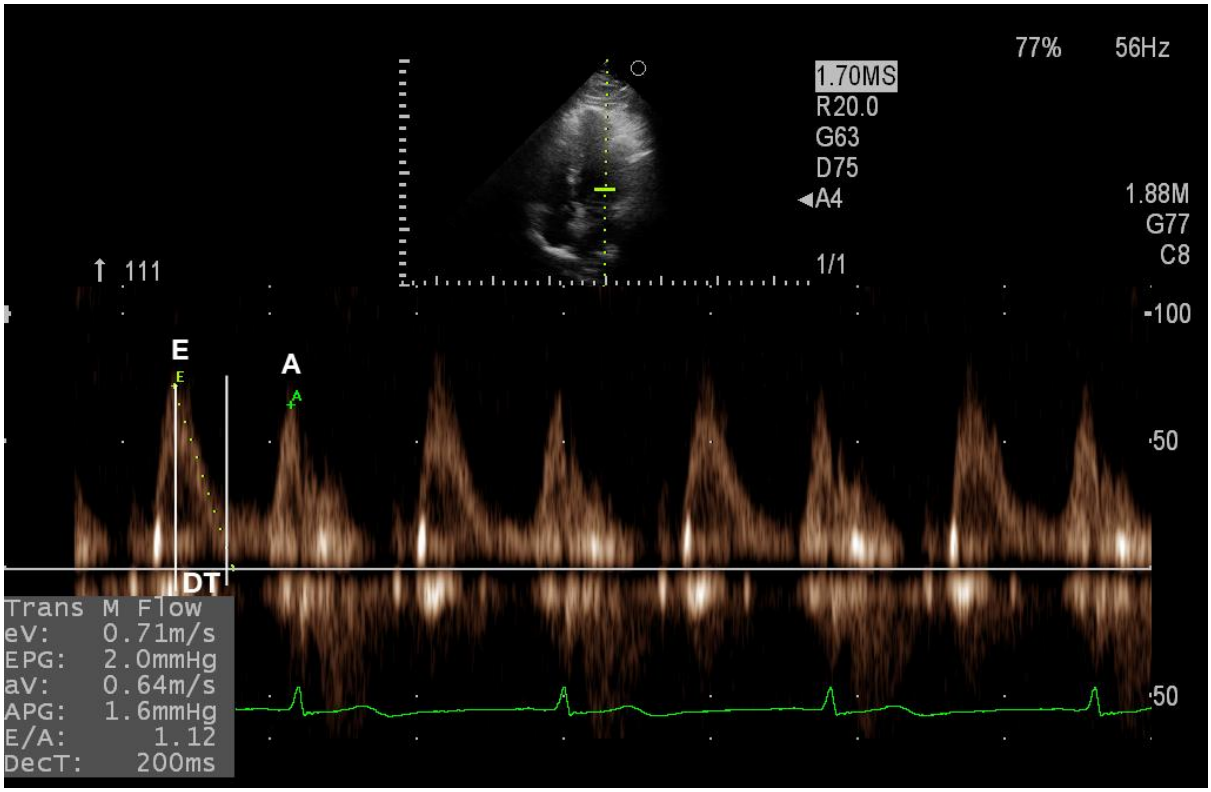

Figure 1 Mitral inflow velocities examination. Pulsed wave Doppler (PW-Doppler) allows the measurement of velocities at the level of the sample volume. Two flow velocity envelopes can be seen during diastole in persons with sinus rhythm: the E-wave, representing the early, passive filling of the left ventricle, and the A-wave, that happens late in diastole, representing the active filling, the atrial contraction.

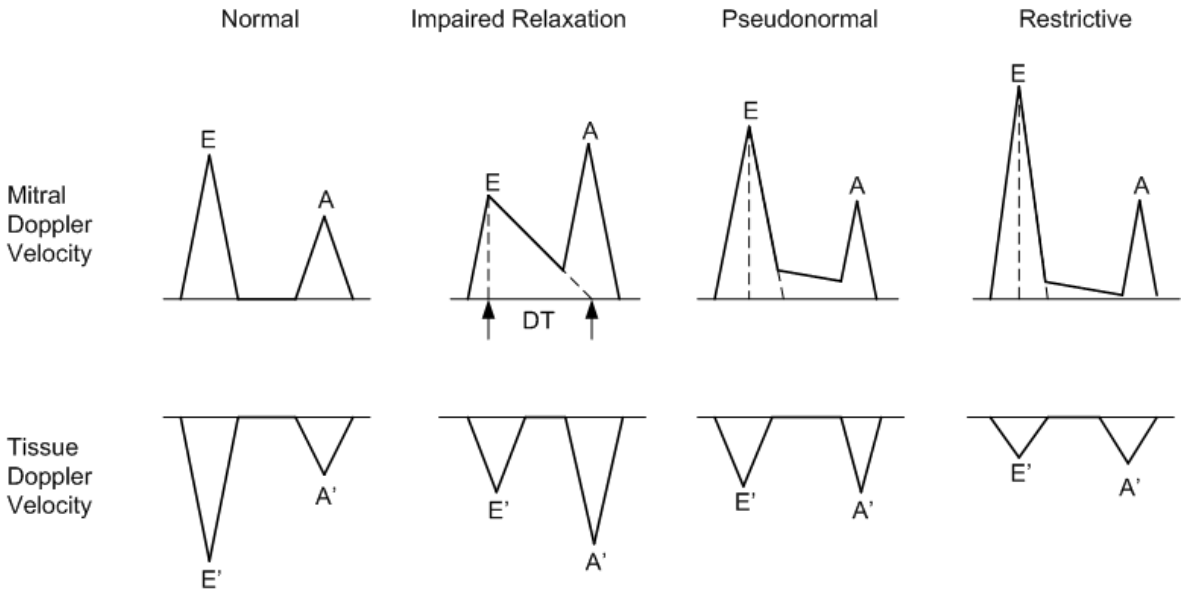

Figure 2 Changes in mitral Doppler velocity and tissue Doppler velocity with LV filling patterns: nomal, impaired relaxation, pseudonormal and restrictive.

1.2 Intra-cardiac Flow Using Echocardiography

Intra-Cardiac flow is useful for evaluating cardiac function as it is the end-result of cardiac myocardial abnormalities. The vortex flow that forms during left ventricular filling is a critical determinant of directed blood flow during ejection, and can offer a novel index of cardiac dysfunction.

Magnetic resonance imaging (MRI) has been used for examining detailed blood flow patterns in the heart and great vessels for a range of clinical conditions [2-4]. In parallel with non-invasive imaging techniques, computational fluid dynamics (CFD) has been used for examining the global flow patterns and pressure distribution since the 1970s and 1980s [5, 6]. The early models were confined to one- or two-dimensions with simplified geometries. With the continuing development of high-performance computing, realistic geometries and fluid-ventricular wall interactions were subsequently incorporated into the CFD models to obtain velocity and pressure distributions in the LV, as well as stress distributions within the wall [7-9].

The integration of current state-of-art real-time MRI flow data and CFD enables visualization of instantaneous three-dimensional flow field and also eliminates the need for velocity scans of the whole heart, thus enabling subject-specific intra-LV flow simulations [10, 11]. However, MRI is relatively expensive and not readily available. Further, this phase contrast velocity mapping technique has limited spatio-temporal resolution, requires additional scans and is time consuming. It is thus not a routinely used technique in clinical settings.

Recent developments in echocardiography enable assessment of intra-cavitary blood flow patterns by tracking the patterns produced by contrast agent particles, called particle imaging velocimetry (echo-PIV) technique [12-14]. However, this technique requires injection of contrast agent, which might lead to serious side effects and has limited velocity range due to tracking algorithm.

Vector flow mapping (VFM) technique has been recently developed to generate flow velocity vector fields by post-processing colour Doppler echo images [15]. In this technique, axial velocity is measured from colour Doppler images, while radial velocity is computed by deconstructing the flow into a basic non-vortical laminar motion and a vortical component. This technique has produced reasonable accuracy when validated with numerical simulation models [16].

In normal subjects, after flow ejection into LV, the direction of flow is reversed towards the apex with a brief appearance of vortex at the early stage of isovolumic relaxation time. The major diastolic anterior vortex develops immediately after the onset of the early diastolic phase. This vortex continued during diastasis, and persists into late LV filling phase. This vortex also persists throughout isovolumic contraction time and dissipates with the opening of the aortic valve and LV ejection [13]

By using echo-PIV and color-Doppler derived VFM, the intra-ventricular vortex flow has been successfully demonstrated and been made applicable in clinical settings, to enable comprehensive assessment of intra-cardiac structure and vortex flow for the detection of pathologically altered flow characteristics and identification of new pathophysiologic mechanisms in the development of cardiac disease.

The quantitative parameters of LV vortex flow are vortex depth (VD) and vortex transversal position (VT). VD represents the vertical position of the centre of vortex relative to the LV long axis, and VT represents the transverse position relative to the posteroseptal axis, as shown below in Fig 3. In the VD and VT configurations, we can measure the parameters of vortex length and vortex width.

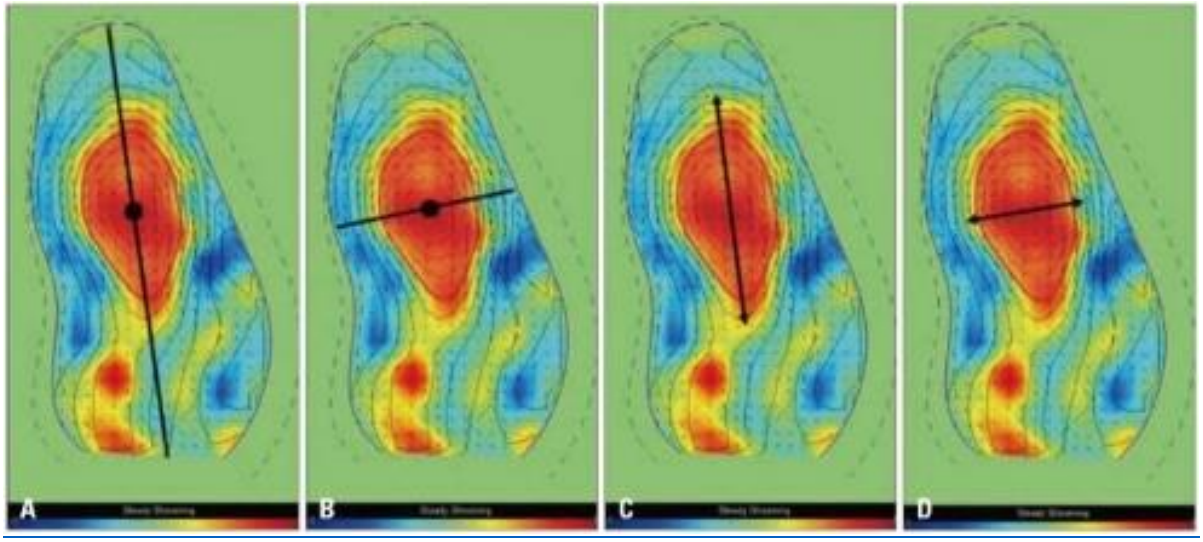

Figure 3 Description of quantitative parameters of the vortex location and shape. Vortex depth (A, black line), vortex transverse position (B, black line), vortex length (C, black arrow), and vortex width (D, black arrow) (Figure adapted from [14])

1.3 Heart Failure with Preserved and Reduced Ejection Fractions

Heart failure (HF), a disease that causes left ventricular (LV) dysfunction, involves high healthcare cost and has high mortality. It is one of the most common diseases in the developed world and is increasingly prevalent in developing countries, especially among the ageing population [17]. HF patients are usually stratified into two groups, based on their LV ejection fraction (EF), which is a commonly used index to assess contractile performance in clinical practice. A patient who has signs and symptoms of HF, while LVEF is normal (>50%), is characterized as HF with preserved ejection fraction (HFPEF). Although the mechanisms of HFPEF are not fully understood, these patients are postulated to have diastolic dysfunction with abnormal LV relaxation during diastolic phase, slow LV filling and increased diastolic LV stiffness, while systolic function remains normal [18, 19]. Thus, earlier, HFPEF was referred to as diastolic HF (DHF), while systolic HF (SHF) corresponded with HF with reduced ejection fraction (HFREF). However, the terms DHF and SHF have been abandoned as diastolic dysfunction has been observed in all symptomatic HF patients, regardless of EF [18].

In recent years, evidence of systolic dysfunction, to a lesser extent, has even been demonstrated in patients with HFPEF. Normal EF, apparently, does not necessarily indicate normal contractility. Regional measures of systolic function assessed by echo tissue Doppler imaging are impaired in HFPEF [20]. Other measures of myocardial contractility, assessed by midwall fractional shortening and particularly our wall-stress-based contractility index, $d\sigma^*/dt_{max}$ formulated as maximal rate-of-change of pressure-normalized wall stress [5] obtained from echo images, are also reduced in HFPEF, compared to healthy subjects [21, 22]. However, end-systolic elastance (Ees), an intrinsic measure of contractile function, defined by the slope and intercept of the end-systolic pressure-volume relationship, is

elevated in HFPEF [21]. From these findings, it is postulated that the same processes such as myocyte hypertrophy and increase in myocardial fibrosis [23] which promote diastolic stiffening also influence systolic stiffness and contribute to reduced myocardial contractility and limited systolic reserve [24].

It is still debatable whether HFPEF and HFREF exist as part of one HF spectrum with HFNEF preceding HFREF or represent two distinct syndromes of HF: HFPEF has concentric remodelling with high LV mass/volume ratio and mainly diastolic dysfunction, while HFREF has eccentric remodelling with low LV mass/volume ratio and a combination of systolic-diastolic dysfunction (HFREF) [25]. The complex mixture of systolic and diastolic dysfunction and variable degrees of LV remodelling underlying HFNEF poses challenges to diagnose and provide pharmacological treatment for HFNEF. In contrast to HFREF, research and clinical trials have not lead to a single effective treatment, and prognosis of HFNEF has remained unaltered for the past 3 decades [26].

1.4 Visualization of Intra-LV Flow Patterns as Outcomes of HFPEF and HFREF for Understanding the Pathophysiological Mechanisms in LV Remodelling Processes

LV myocardial structural remodelling processes in HFNEF and HFREF follow significantly different underlying mechanisms. In HFNEF, prominent cardiomyocyte hypertrophy is observed [27]. Cardiomyocyte diameter in HFNEF increases significantly, in contrast to minor increase in cardiomyocyte diameter in tandem with the dilated LV. Besides, although there is increased myocardial collagen deposition in both HFNEF and HFREF, the breakdown and turnover of the extracellular matrix are different [27]. This explains the different cardiomyocyte remodelling patterns: concentric hypertrophy in HFNEF and eccentric hypertrophy in HFREF. The passive force of cardiomyocytes in HFNEF is also higher than that of cardiomyocytes in HFREF, accounting for relatively more elevated LVEDP and increased myocardial stiffness in HFNEF compared to HFREF [27].

Further, other mechanisms underlying HFNEF include ventriculo-vascular coupling, chronotropic incompetence, LA dilatation, volume overload and pulmonary arterial hypertension, which can contribute to HF in HFNEF patients. All these concomitant structural and functional changes can affect the haemodynamics inside the LV chamber. The development of intra-LV flow patterns is the result of how (i) the LV myocardium passively responds to left atrial ejection of blood into the LV to result in diastolic filling flow patterns and pressure during diastolic filling, and (ii) then actively contracts to generate intra-LV flow patterns and pressure during systole to direct blood out of the LV. Therefore the visualization of these diastolic and systolic intra-LV flow patterns can provide a wealth of dynamic information for understanding the intra-LV flow outcomes of the pathophysiological mechanisms in the LV remodelling processes.

In this regard, in our earlier chapter 4, we have described in detail the effect of cardiomyopathy on LV remodelling process in terms of curvedness and sphericity indices. Then in our chapter 10, we have analysed intra-LV flow and relative pressure distributions obtained by fluid-ventricular wall interactions from angiographic X-ray images of sequential LV endocardial boundaries in patients with myocardial disorders.

Herein, we apply **Vector flow mapping** (VFM) technique, to obtain intra-LV flow patterns for patients with HFNEF, HFREF and normal subjects, in order to characterize the LV performance outcomes of normal subjects and heart failure patients. This chapter is an

extension of our earlier work reported in our paper: Intra-Left Ventricular Flow Distributions in Diastolic and Systolic Phases, based on Echo Velocity Flow Mapping of Normal subjects and Heart Failure Patients, to Characterize Left Ventricular Performance Outcomes of Heart Failure, *Journal of Mechanics in Medicine and Biology*, Vol. 12, No. 5, World Scientific Publishers [28].

2. Clinical Study Methodology to Determine Intra-LV Flow Patterns for HF Patients and Normal Subjects

2.1. Subjects recruitment

Patients who had signs and symptoms of congestive HF based on the modified Framingham criteria [29] were recruited for this study. They subsequently underwent echo scan for stratification into HFNEF (based on LVEF $\geq$ 50%) and HFREF (LVEF <50%). Normal subjects, who had no history of heart disease or hypertension, were also recruited. For each group, 2 age- and sex-matched subjects were chosen. The study procedure was approved by the institutional ethical committee.

2.2. Echo data acquisition

All subjects underwent echo scans (Alpha10, Aloka). The LVEF was measured from M-mode images at the parasternal long-axis view using standard methodology. Mitral E and A velocities deceleration time (DT), systolic (PVs) and diastolic (PVd) pulmonary vein velocities were measured from pulsed wave Doppler images, while the septal E' velocity was measured from pulsed tissue Doppler images. These echo measurements assess LV diastolic function.

Colour Doppler flow images were captured at the 3-chamber view for visualization of both inflow through mitral valve and outflow into the aorta.

2.3. Vector Flow Mapping (VFM) analysis

Intra-LV flow was determined using the VFM analysis package (DAS-RS1). In this technique, colour Doppler velocity (axial velocity, **u**) profile was analysed across an arc (refer Figure 4) at each echo depth. The Doppler velocity **u** along the beam line is composed of basic non-vortical laminar flow ($\mathbf{u_b}$) and vortex flow ($\mathbf{u_v}$) components. If the Doppler velocity profile on the arc has both negative and positive fractions, it is considered to be a combination of non-vortical and vortical laminar flows.

The vortex feature is assumed to be bilaterally symmetric, so that the negative and positive components of $\mathbf{u_v}$ perpendicular to the arc negate each other (Figure 4). The basic flow component $\mathbf{u_b}$ is computed as:

$$\mathbf{u_b} = \mathbf{u} - \mathbf{u_v} \quad (1)$$

The stream function $\psi(r, \theta)$expresses the flux of the 2D flow. The vortex flow velocity components u_v and $\mathbf{v_v}$ can be obtained in terms of ψ , as:

$$\mathbf{u_v} = \frac{1}{r}\frac{\partial \psi}{\partial \theta} \quad (2)$$

$$\mathbf{v_v} = -\frac{\partial \psi}{\partial \theta} \quad (3)$$

wherein r and θ are radial and angle coordinates expressing the location of the pixel.

From equation (2), the stream function ψ can be expressed as:

$$\psi(r, \theta) = \int_0^{\theta} \mathbf{u_v}(r, \theta) r d\theta \quad (4)$$

As the vortex feature is assumed to be bilateral symmetric, the flux calculated by the positive and negative components of $\mathbf{u_v}$, which intersect perpendicularly with the integration arc, negate each other.

The radial vortex flow component $\mathbf{v_v}$ can be computed from equation (3).

To compute basic flow component, Ohtsuki and Tanaka [15] have proposed a flow function $F(r,\theta)$ to describe a non-vortical laminar flow within a defined plane as:

$$F(r,\theta) = \int_0^{\theta} \mathbf{u_b}(r,\theta) r d\theta \tag{5}$$

To find the direction of flow vectors in the basic flow component, $F(r,\theta)$ is normalized by the total flow rate in the basic flow component across an arc, as:

$$F_n(r,\theta) = \frac{\int_0^{\theta} \mathbf{u_b}(r,\theta) r d\theta}{\int \mathbf{u_b}(r,\theta) r d\theta} \tag{6}$$

The contour line connecting points that have the same value of $F_n(r,\theta)$ indicates the direction of flow vectors in the basic flow component. The radial basic flow component $\mathbf{v_b}$ can then be found as:

$$\mathbf{v_b} = \mathbf{u_b} tan\theta \tag{7}$$

Flow velocity $\mathbf{U}(r,\theta)$ can be calculated by:

$$\mathbf{U}(r,\theta) = \big(\mathbf{u_b}(r,\theta) + \mathbf{u_v}(r,\theta)\big)\mathbf{i}(r,\theta) + \big(\mathbf{v_b}(r,\theta) + \mathbf{v_v}(r,\theta)\big)\mathbf{j}(r,\theta) \tag{8}$$

where $\mathbf{i}(r,\theta)$ and $\mathbf{j}(r,\theta)$ are the unit vectors in the axial and radial direction, respectively, at point (r,θ). As illustrated in Fig 4, $\mathbf{u_b}$ and $\mathbf{u_v}$ are in the Doppler beam direction (axial), while $\mathbf{v_b}$ and $\mathbf{v_v}$ are in the direction perpendicular to the Doppler beam (radial)

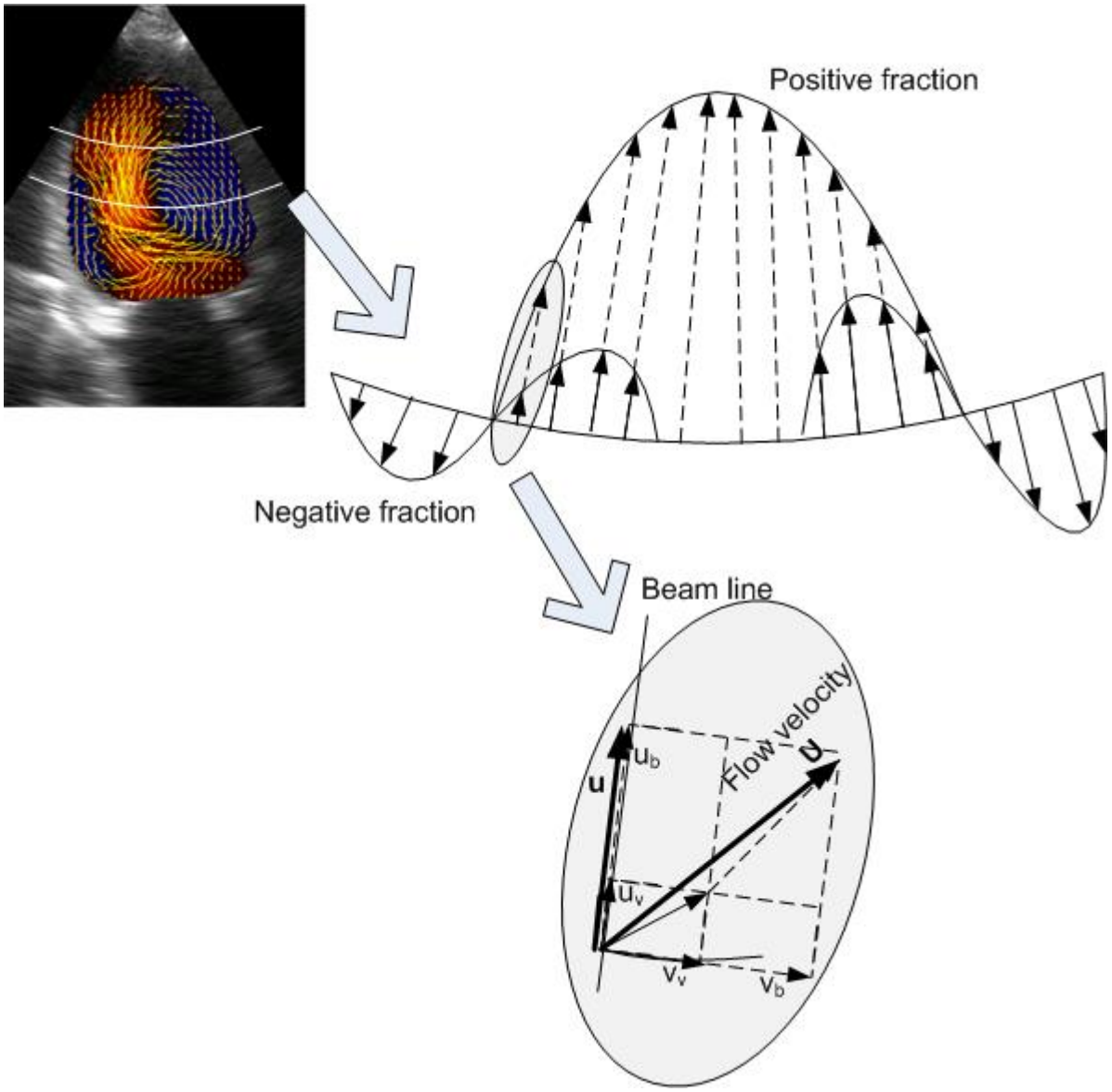

Figure 4 Velocity generated by VFM along an arc at each echo depth with a combination of single laminar flow and vortex flows (Top left). Colour Doppler flow data are separated into basic and vortex flow components so that vortex flow component is bilaterally symmetrical on each arc (Top right); At a given pixel, colour Doppler velocity u along the beam line is a sum of its vortex flow component u_v and basic flow component u_b. The vortex flow component consists of colour Doppler velocity u_v and radial velocity v_v. Likewise, the basic flow component consists of colour Doppler velocity u_b and radial velocity v_b. Flow vector is the sum of flow vectors of basic and vortex flow components (Bottom).

The velocity vector distributions throughout the cardiac cycle are then analyzed and compared among all subjects. The LV outflow rates during systole and inflow rates during diastole were determined by computing the flow rates passing through a line drawn across the LV outflow tract (LVOT) during systole and a line across the mitral valve (MV) annulus during diastole (refer to fig 5).

Fig 5 illustrates measurement of maximal flow rate into the aorta using velocity flow mapping (VFM). The figure on the left shows the Velocity vector distribution in the LV

during systole; therein, the arrows denote velocity vectors, and the red dots indicate heads of the arrows; a line is drawn at the LVOT to determine the maximum flow rate ejected into the aorta. In the figure on the right, we can see the Flow profile through the line drawn at LVOT at a time instant.

2.4. LV Contractility Index based on LV wall stress

We want to define a contractility index in order to characterize HFREF (systolic heart failure) patients, who (due to myocardial disease) have depleted contractility. For this purpose, we have previously developed a LV wall-stress based contractility index, based on the premise that in systole it is the active wall stress (produced by the actin and myosin contracting components of the myocardial structural unit) that in turn produces the intra-LV pressure, leading to the traditional contractility index dP/dt_{max}.

Our wall-stress-based contractility index, $d\sigma^*/dt_{max}$, defined as a maximal rate-of-change of pressure-normalized wall stress, has been proposed in our paper [22] as an intrinsic measure of contractile function. This index has been shown to have a good correlation with dP/dt_{max}, which is considered as a "gold standard" index for assessing myocardial contractility, and Ees, and can be determined non-invasively. We, therefore, apply this index to assess contractile performance of all subjects in this study.

This $d\sigma^*/dt_{max}$ index is formulated as:

$$d\sigma^*/dt_{max} = 1.5 \times \frac{dV/dt_{max}}{MV} \tag{9}$$

where dV/dt_{max} is maximal flow rate into the aorta, measured at the LVOT using VFM (Figure 5), and MV is the myocardial volume, calculated as a quotient of LV mass, determined from M-mode images using Devereaux's method, and myocardial density (assumed 1.05g/ml).

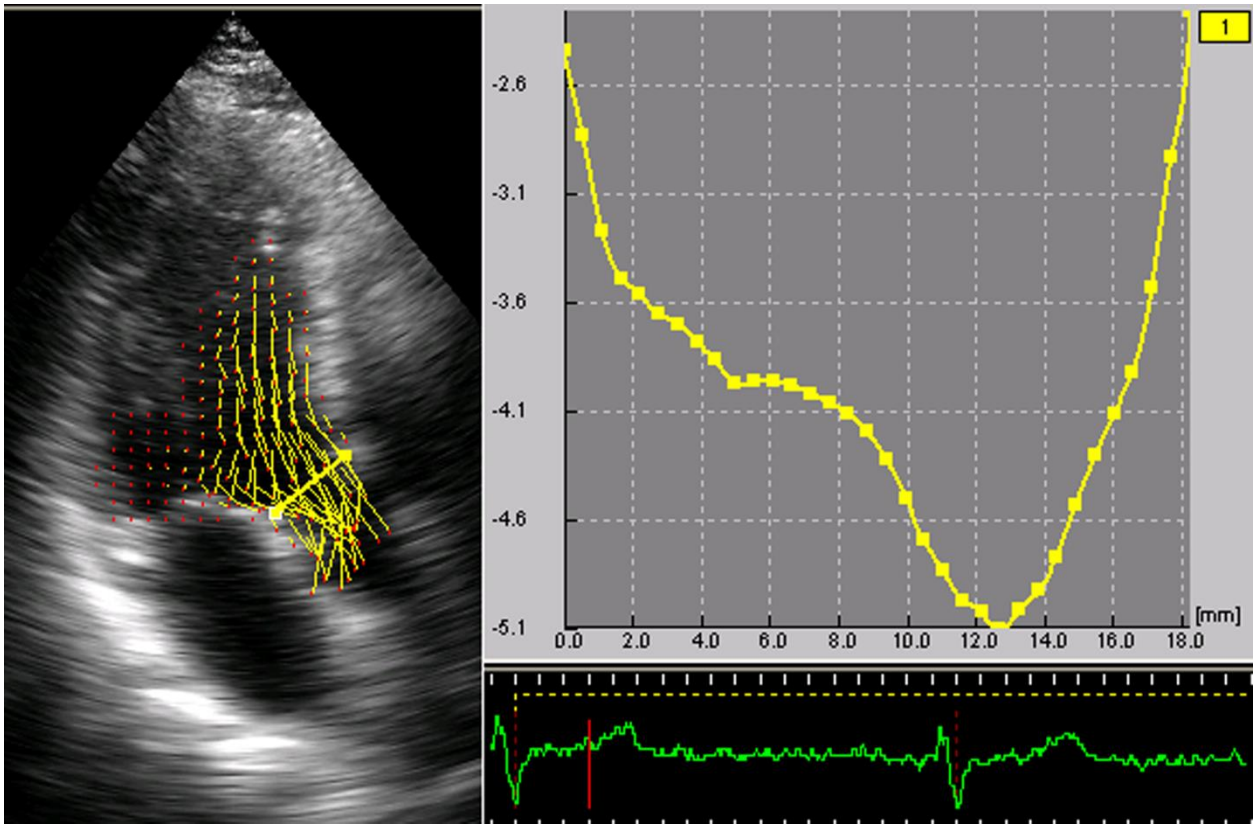

Figure 5: Measurement of maximal flow rate into the aorta using velocity flow mapping (VFM). (Left) Velocity vector distribution in the LV during systole. Arrows denote velocity vectors. Red dots indicate heads of the arrows. A line was drawn at the LVOT to determine the maximum flow rate ejected into the aorta. (Right) Flow profile through the line drawn at LVOT at a time instant.

3. Results of the Intra-LV VFM, to characterize the LV performance in Heart Failure

3.1 Subjects' clinical characteristics and echo parameters

Clinical characteristics and echo parameters of 4 HF subjects and 2 age- and sex-matched healthy controls are shown in Table 1. The HFNEF1 and HFNEF2 are HF patients with normal EF. HFREF1 and HFREF2 are HF patients with reduced EF. The Normal1 and Normal2 are normal subjects with no history of cardiac problems. All HF patients were on hypertensive medication. Subject HFNEF1 had elevated systolic blood pressure while the rest are normotensive. LV hypertrophy was seen in subjects HFREF1 and HFNEF2. Dilated LA was observed in subjects HFREF1, HFREF2 and HFNEF2.

In all HF subjects, the clinical echo data has suggested abnormal filling patterns (either restrictive or pseudo-normal), with increased E/A ratio. In subjects HFREF1 and HFREF2, there was decreased deceleration time DT.

All HF patients had raised E/E' ratio >15, associated with increased filling pressure.

Subject	Age	Gender	LVEF (%)	E/A	E/E'	DT (ms)	PVs/PVd
HFNEF1	52	Male	64.7	2.5	19.5	210	0.90
HFREF1	53	Male	26.6	1.3	26.9	120	NA
Normal1	51	Male	60.4	0.8	5.9	184	1.27
HFNEF2	66	Female	63.3	2.7	27.7	216	0.63
HFREF2	65	Female	22.6	3.6	21.8	68	NA
Normal2	67	Female	60	0.8	6.6	168	1.61

Table 1. Subject's clinical characteristics and echo parameters.

In general, restrictive filling pattern, with increased E/A ratio and decreased DT, were seen in patients with HFREF. Pseudo-normal filling patterns were observed in patients with HFNEF. Normal subjects had reversed E/A ratios (<1), which are common features in aging subjects.

3.2 Diastolic flow patterns

The diastolic flow patterns are shown for each of the 6 subjects HFNEF1, HFREF1, Normal1 (in rows 1, 2 & 3 of Figure 6A) and HFNEF2, HFREF2, Normal2 (in rows 1, 2 & 3 of Figure 6B).

After the mitral valve opens, in the rapid filling phase (frame 1), straight flow is seen to rush into the LV from the LA. Circulating flow patterns are seen at the anterior and posterior walls of the LV in all subjects, except in subject Normal2.

As inflow reduces its speed (frame 2), the circulating flow patterns are seen to become bigger. The circulating flow is seen to be more prominent at the anterior wall.

In the diastasis phase (frame 3), marked by P-wave on ECG, the flow patterns are seen to be different among the subjects. In subject HFNEF1, the flow is seen to be circulating in the LV with no inflow. In both subjects HFREF1 and HFREF2, the flow from LA is seen to be continuing to enter LV, with 2 circulating flow patterns seen at the anterior and posterior walls. In contrast, there is hardly any movement of blood in LV of subjects Normal1 and HFNEF2. In Normal2, continuous flow from LA to LV is seen, with a circulating flow at the anterior wall.

At atrial contraction (frame 4), after the P-wave on ECG, as LA contracts, the flow starts to again enter the LV in Normal1 and HFNEF2, after a period of no inflow into the LV. In the rest of the subjects, the flow from LA to LV is observed to have profound circulating flow patterns at the anterior wall. . These circulating flow features remain until the end of atrial contraction (frame 5).

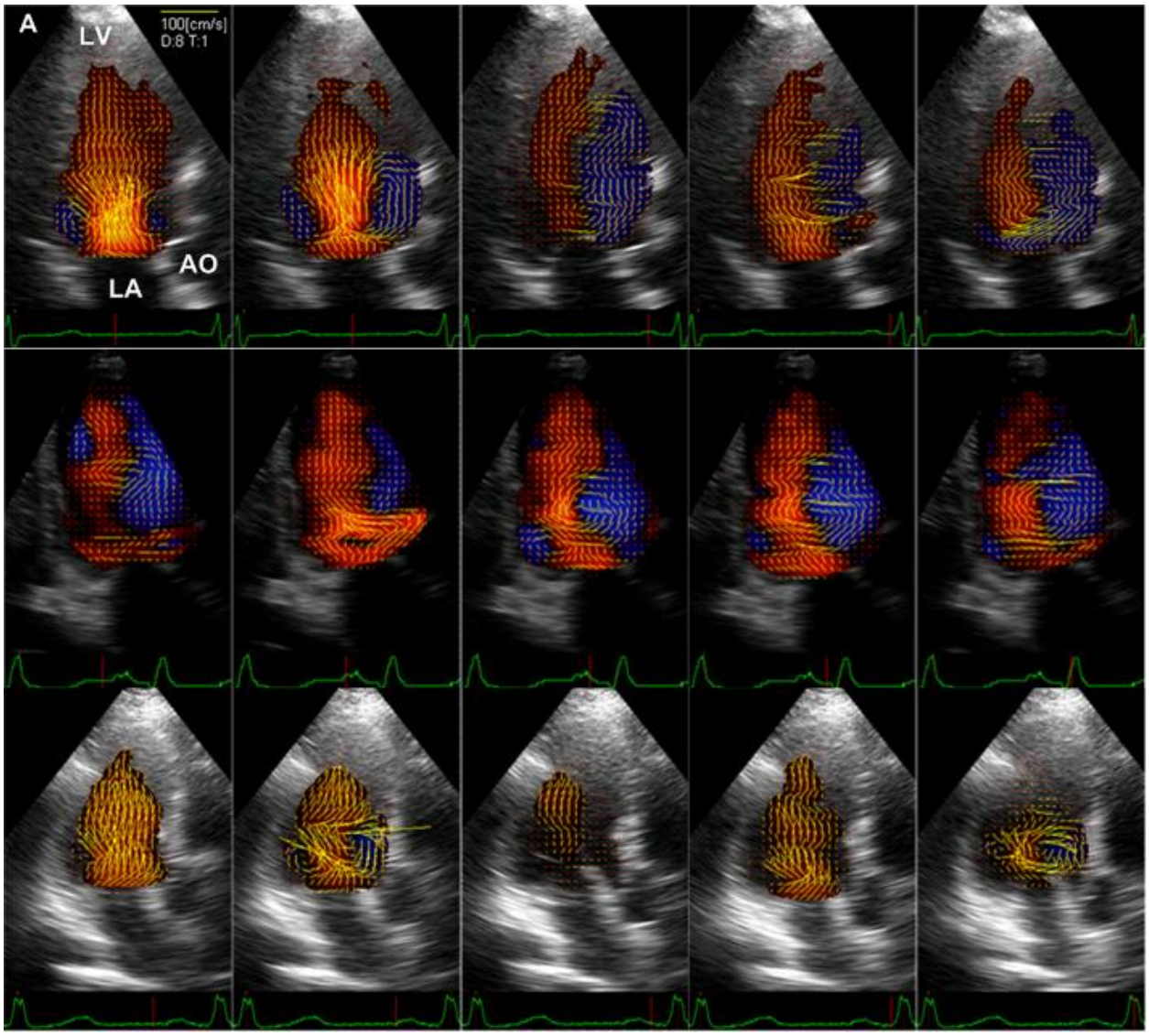

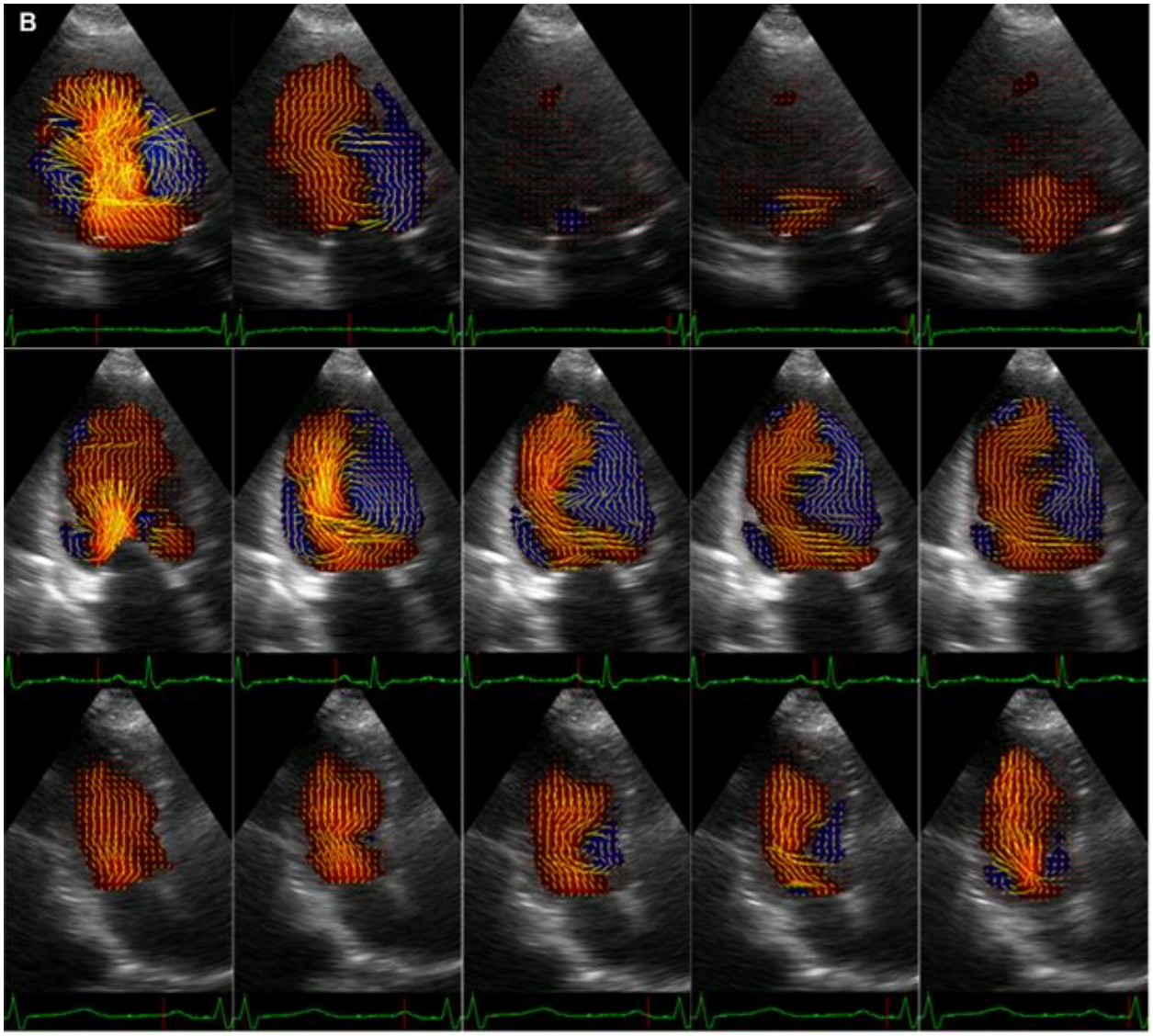

Figure 6 Diastolic flow patterns of age- and sex-matched subjects (A) HFNEF1, HFREF1 and Normal1; (B) HFNEF2, HFREF2 and Normal2 at (from left to right) the start of rapid filling (frame 1), late rapid filling (frame 2), diastasis (frame 3), start of atrial contraction (frame 4), and end of atrial contraction just before mitral valve closes (frame 5). Inflow towards the apex is represented in red color, outflow towards the aorta (AO) is represented in blue color.

The flow rates versus time (corrected for heart rate) of all the subjects during diastole phase, from the start of aortic valve closure to mitral valve closure, are shown in Figure 7.

In both HFNEF patients, prolonged diastasis phase (period of no inflow) is to be seen.

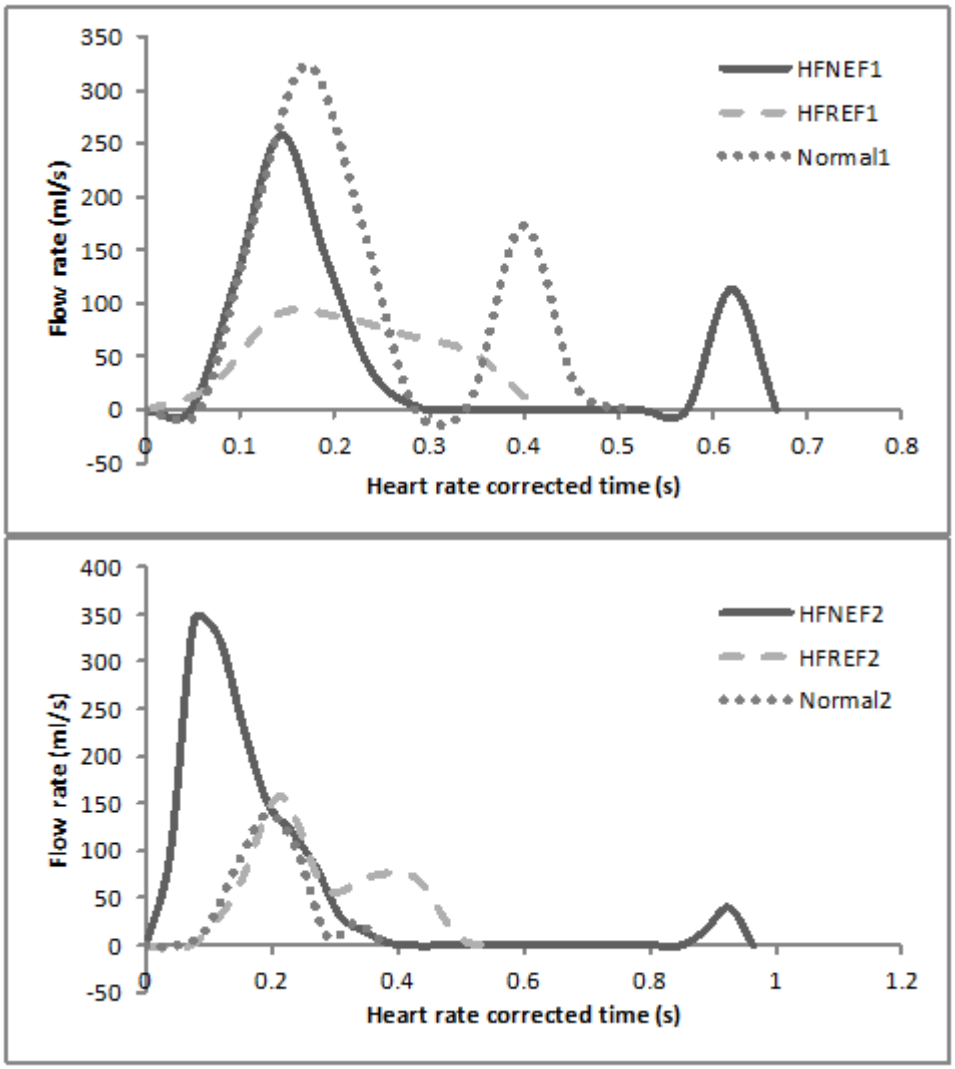

Figure 7 Flow rates from the LA into the LV versus time (corrected for heart rate) of (top) HFNEF1, HFREF1 and Normal1; and (bottom) HFNEF2, HFREF2 and Normal2, during diastole.

3.3 Systolic flow patterns

Systolic flow patterns are shown for each of the 6 subjects: HFNEF1, HFREF1, Normal1 (in rows 1, 2 & 3 of Figure 8A) and HFNEF2, HFREF2, Normal2 (in rows 1, 2 & 3 of Figure 8B).

In Fig 8, flow towards the aorta is illustrated in blue color, and flow towards the apex is illustrated in red color. At isovolumic contraction (frame 1), LV contraction produced recirculating flow patterns and directed flow towards the aortic valve. At early systole (frame 2), flow is seen to be pouring out of the LV; however, recirculating flow is observed in all subjects. The flow gets ejected to the aorta rapidly at mid systole (frame 3) and is gradually reduced at the end of systole (frame 4). In subjects HFNEF1, HFREF1 and HFREF2, the abnormal recirculating flow pattern, formed during isovolumic contraction, is seen to remain until the end of the systolic phase.

At isovolumic relaxation (frame 5), there is observed to be virtually no flow in the LV of HFNEF patients and normal subjects. However, some flow movement is still present in HFREF patients.

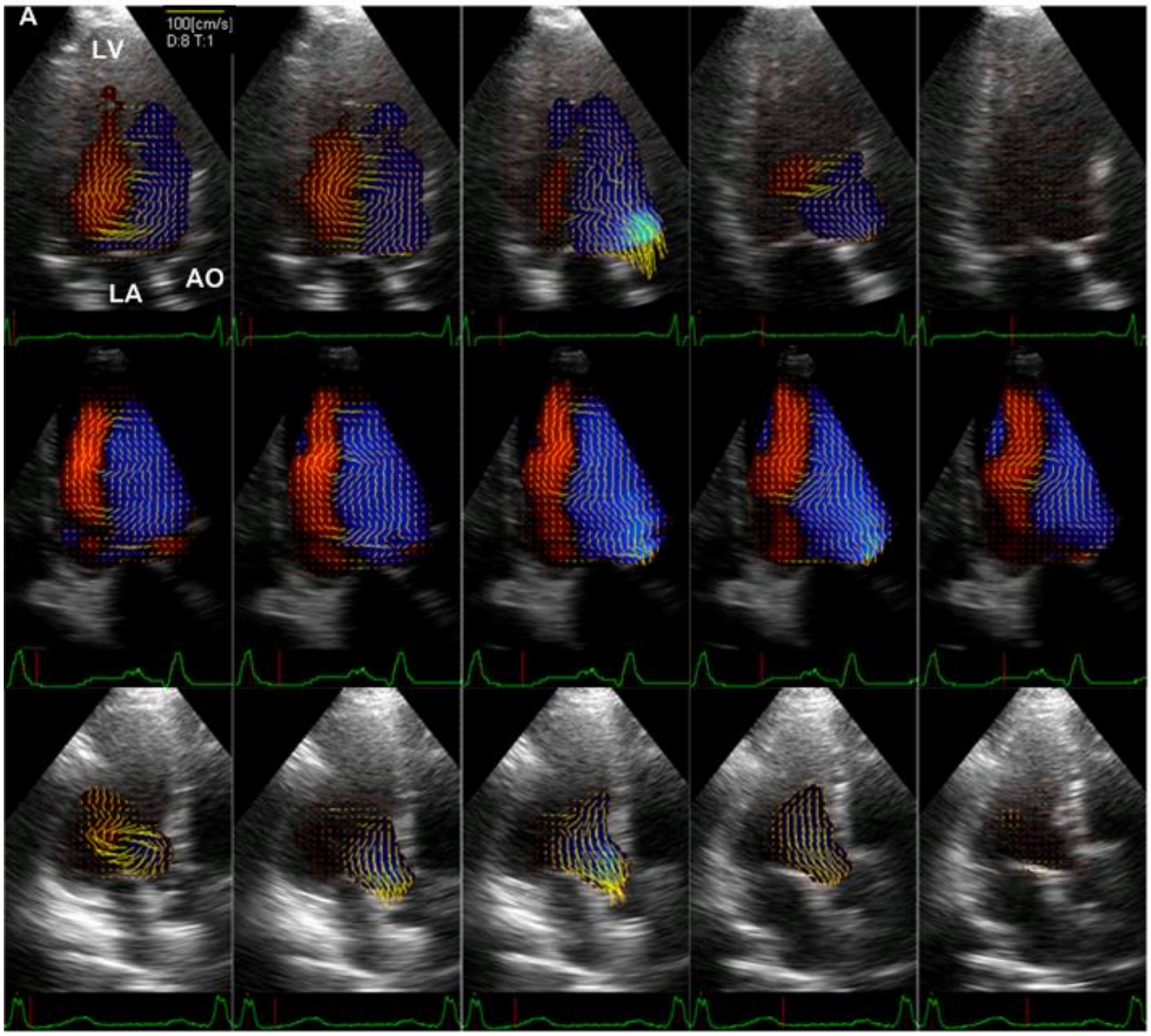
A
LV
100[cm/s]
D:8 T:1
LA
AO

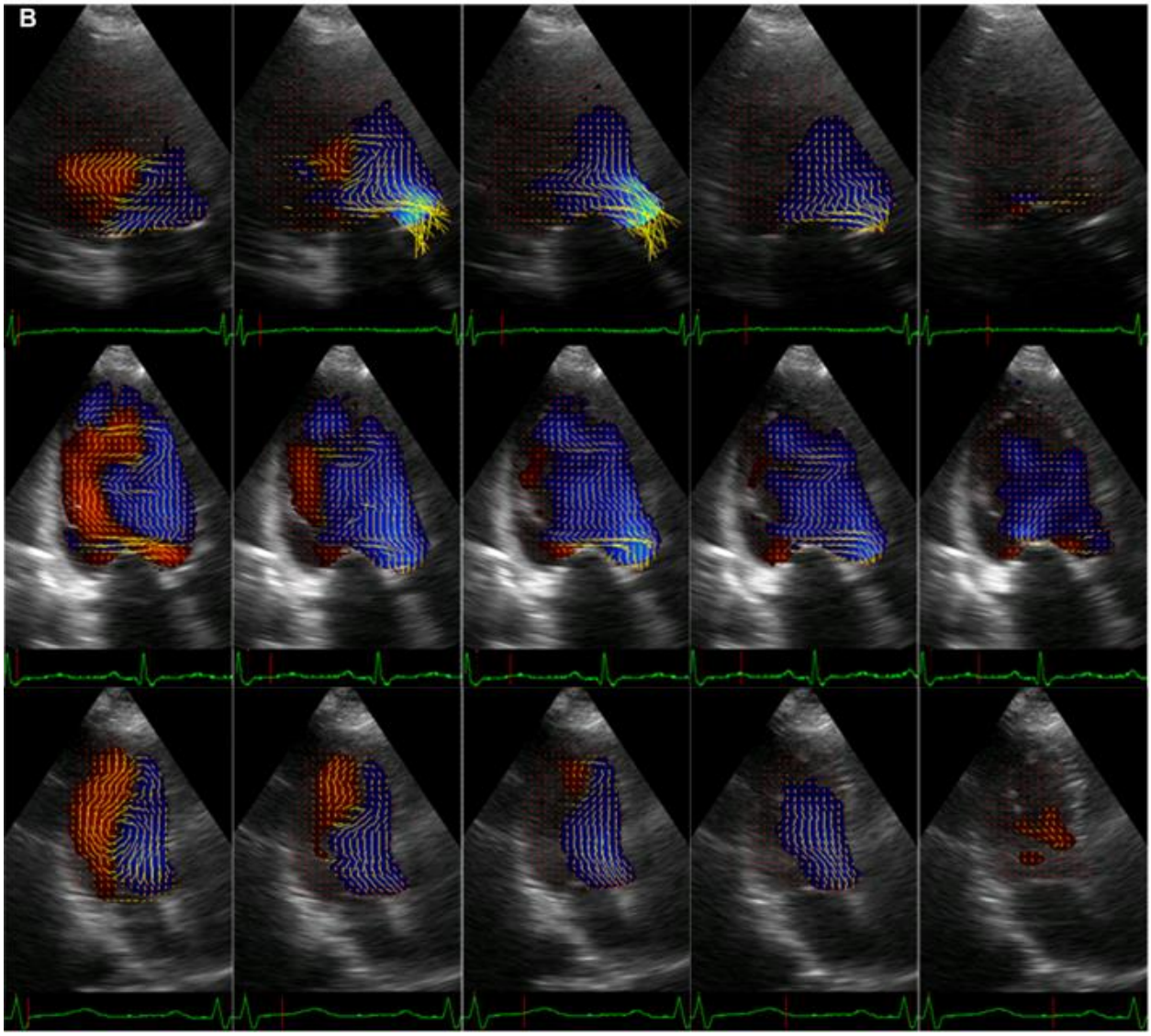

Figure 8 Systolic flow patterns of age- and sex-matched (A) HFNEF1, HFREF1 and Normal1 subjects; (B) HFNEF2, HFREF2, and Normal2 subjects at (from left to right) isovolumic contraction (frame 1), early systole (frame 2), mid systole (frame 3), end systole (frame 4) and isovolumic relaxation (frame 5). Blue indicates flow towards the aorta. Red indicates flow toward the apex. Arrow represents velocity flow vector. Red dot indicates the head of the arrow.

In general, persistent recirculating flow patterns are seen during the ejection phase in patients with HFREF. At isovolumic relaxation, while there is virtually no intra-LV flow in HFNEF patients and normal subjects, flow movement is still present in the LV of HFREF patients.

The instantaneous flow rates ejected into the aorta of 6 patients are shown in Figure 9. To correct for heart rate, the time intervals were divided by $\sqrt{\text{R-R}}$, based on Bazette's formula, which normalizes the heart rate to 60 beats/minute.

Subject HFNEF1 is shown to have a higher peak flow rate (341.1 ml/s), compared to HFREF1 (270.5 ml/s) and Normal1 (320.8 ml/s). A steeper slope of the flow rate curve of

subject HFNEF1 is seen in the graph, indicating a faster rate-of-change of flow rate, compared to HFREF1 and Normal1.

Subject HFNEF2 is shown to have a higher peak flow rate (255.4 ml/s) and faster rate-of-change of flow rate compared to HFREF2 (87.6 ml/s) and Normal2 (151.6 ml/s).

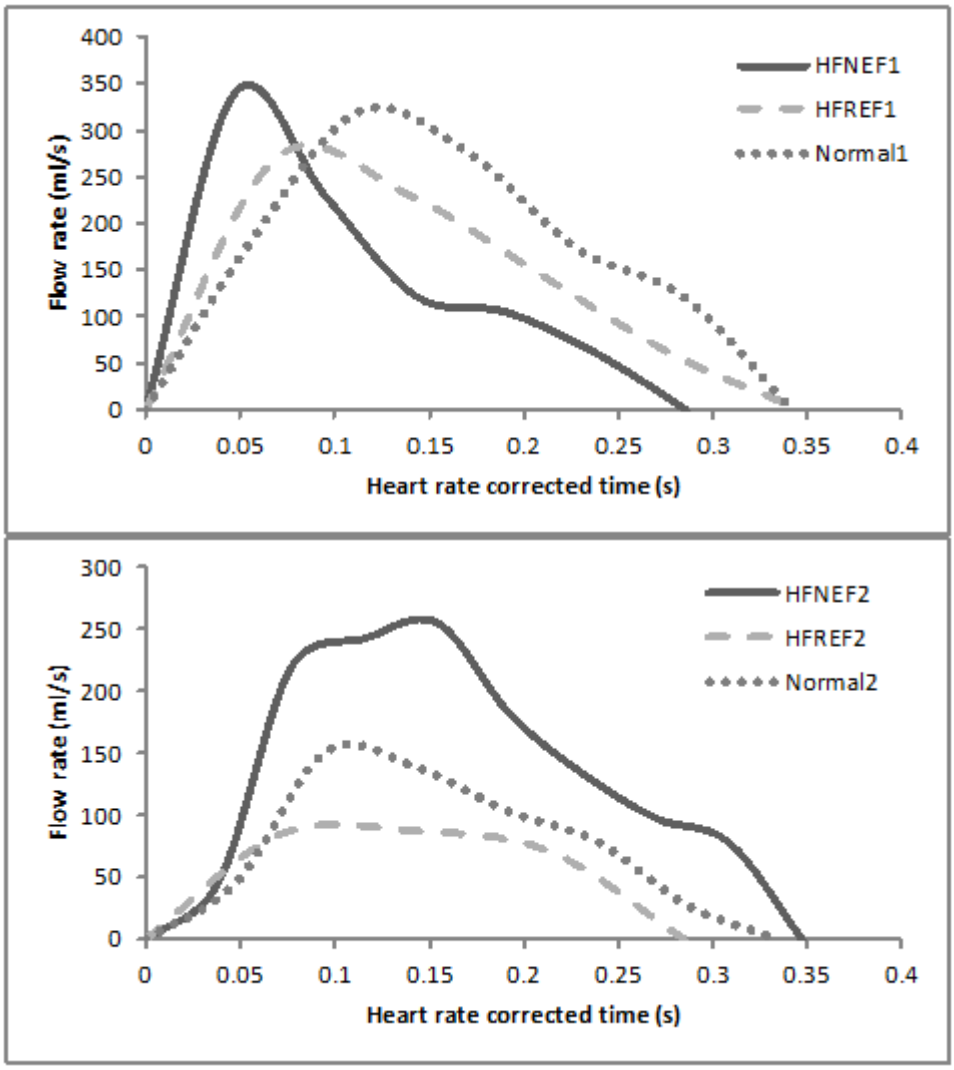

Figure 9 Flow rate from LV into the aorta versus time (corrected for heart rate) of (top) HFNEF1, HFREF1 and Normal1; and (bottom) HFNEF2, HFREF2 and Normal2, during systole.

3.4. Contractility Index, Peak Inflow and Outflow Rates of all Subjects

Table 2 lists the values of the LV myocardial volume, and the calculated values of the contractility index, peak systolic outflow rate, peak filling flow rate, peak atrial contraction flow rate and Doppler A velocity.

Subject	$d\sigma^*/dt_{max}$ (s^{-1})	Myocardial Volume	Peak systolic	Peak rapid	Peak atrial contraction	Doppler A

		(ml)	outflow rate (ml/s)	filling flow rate (ml/s)	flow rate (ml/s)	velocity (cm/s)
HFNEF1	4.41	116	341.1	258.0	113.6	37.4
HFREF1	1.80	285	270.5	89.6	NA	56
Normal1	4.31	111	320.8	323.7	172.9	61
HFNEF2	1.31	292	255.4	344.8	40.3	42.8
HFREF2	0.62	213	87.6	158.0	73.2	34
Normal2	3.34	68	151.6	138.6	23.7	70

Table 2. Contractility index, peak outflow and inflow rates of all subjects

As shown in Table 2, there is marked reduction of $d\sigma^*/dt_{max}$ in patients with HFREF; correspondingly, there is also marked reduction of peak systolic outflow rate in HFREF patients.

Despite normal values of clinical pulsed Doppler mitral A velocity (between 30 – 70 cm/s), low flow rates during atrial contraction are observed in subjects HFREF1, HFNEF2, HFREF2 and Normal2. The A velocities are 56 cm/s (HFREF1), 42.8 cm/s (HFNEF2), 34 cm/s (HFREF2) and 70 cm/s (Normal2).

As seen in Table 2, a lower value of the contractility index $d\sigma^*/dt_{max}$ is observed in subject HFNEF2, compared to the normal subject with same age and gender, with higher peak outflow rate and increased myocardial volume. There is no difference in $d\sigma^*/dt_{max}$ between HFNEF1 and Normal1. HFREF patients are seen to have lower peak flow rate and lower $d\sigma^*/dt_{max}$ compared to HFNEF patients and normal subjects of the same age and gender.

4. Discussion and Conclusion

4.1 Intra-LV Flow patterns variations

Herein, the VFM analysis has provided similar common flow patterns to those obtained from combination of CFD and MRI [11] and contrast echo [13]. Even though colour Doppler images have much lower temporal resolution compared to two-dimensional echo images used for echo PIV, the current frame rates of 20-30 frames/seconds are quantifiably comparable to those obtained by phase-contrast MRI. This technique, thus, has great potential in clinical applications, as colour Doppler echo is widely used in routine clinical practice.

In this study, we have demonstrated the use of VFM technique to visualize blood flow patterns in HF patients and normal subjects. Abnormal circulating flow patterns, which were observed at late systole and from late rapid filling phase to diastasis in HF patients, may suggest a stiff LV, which is resistant to expansion and contraction.

4.2 Contractility Index Variations

To assess the LV contractile function, the pressure-normalized wall stress based contractility index, $d\sigma^*/dt_{max}$, is used in this study. In systole, the wall stress, which is generated by sarcomere contraction and results in the development of pressure, can be considered as an intrinsic contractile indicator. The contractile index $d\sigma^*/dt_{max}$is markedly reduced in HFREF patients, compared to HFNEF and normal subjects of the same age and sex. This confirms impaired contractile function in HFREF patients.

In HFNEF patients, the contractile index $d\sigma^*/dt_{max}\ is$ reduced in the case of HFNEF2, compared to Normal2, while for HFNEF1 it remains similar to that of the normal subject Normal1.

The contractility index $d\sigma^*/dt_{max}$ is formulated as the quotient of maximal flow rate into the aorta and myocardial volume. In both HFNEF cases, the outflow rates are higher than those of normal subjects. However, in HFNEF2, the myocardial volume is increased due to LV hypertrophy (refer to Table 2), probably to compensate for the increase in stroke volume. Due to this compensatory mechanism, the contractile performance assessed by pressure-normalized wall stress $d\sigma^*/dt_{max}$ is seen to be reduced.

4.3 Flow Rates into and out of LV

The peak flow rates out of LV are reduced in both cases of HFREF, which are associated with reduced contractile function. The peak LV outflow rates of patients with HFNEF, on the other hand, are increased compared to those of normal controls. The mechanisms underlying this observation are not quite clearly understood.

Even though diastolic dysfunction is present in both HFNEF and HFREF patients [30], different patterns of flow distribution in the diastolic phase are seen in the case of these two sets of patients. In HFREF patients, the peak inflow rates in rapid filling phase are reduced. It is noticed that during isovolumic relaxation, as both the valves were closed and LV continues to relax, the circulating flow patterns are still present. This might be due to impaired elastic recoil, influenced by reduced contractility. Intraventricular pressure, thus, may still be high in these patients during isovolumic relaxation. This may, therefore, affect the LV transmural pressure, and hinder LV filling.

On the other hand, HFNEF patients have prolonged diastasis phase. In HFNEF1, the circulating flow, formed at the start of rapid filling, becomes larger and has lasted throughout the diastasis phase. This may suggest high LV stiffness which is resistant to LV expansion. In HFNEF2, the LA dilation, which is evident from echo scan and is possibly resulting from increased filling pressure due to LV hypertrophy, may be the cause of delayed atrial contraction.

The discordance between normal pulsed Doppler mitral A velocity and low atrial contraction inflow rate into the LV might be due to the location of the velocity sample, which is placed at the tip of the mitral valve. The Doppler velocity measured at this location might be affected by the concomitant circulating flow, which is formed in the LV cavity during rapid filling phase, as shown in Figure 8. Therefore, Doppler A velocity may overestimate the actual contribution of atrial contraction to LV filling.

Thus, in future studies, both LV myocardial elastance, LV ejection force (which is an outcome measure of LV contractility) and LA ejection force (which is an outcome based measure of LA contractility) need to be determined, in order to fully understand the

mechanisms behind (i) different systolic flow patterns diastolic flow patterns and characterize systolic dysfunction, and (ii) various type of diastolic flow patterns and diastolic dysfunction.

4.4 Intra-LV Pressure Gradients

Also, by applying Navier-Stokes equation, intraventricular LV pressure gradients can be calculated from the flow velocity, as performed by Subbaraj et al [11]. This will, thereby provide information on both the instantaneous intra-cavitary LV blood flow velocity field as well as the intra-LV pressure field, and the relationship between velocity distribution and pressure distribution. This can lend enhanced insight into the outcomes of efficiency of LV contraction and relaxation.

Terminologies

E: peak flow velocity at rapid filling phase, measured from pulsed Doppler echo.

A: peak flow velocity at atrial contraction phase, measured from pulsed Doppler echo.

DT: deceleration time, measured from peak to end of rapid filling phase from pulsed Doppler echo.

E': peak myocardial velocity, measured at the septal mitral annulus from pulsed tissue Doppler echo.

PVs: peak systolic flow velocity from pulmonary vein to LA, measured from pulsed Doppler echo.

PVd: peak diastolic flow velocity from pulmonary vein to LA, measured from pulsed Doppler echo.

$\mathbf{u_b}$, $\mathbf{u_v}$: basic non-vortical laminar flow and vortex flow components of Doppler velocity, respectively.

$\mathbf{v_b}$, $\mathbf{v_v}$: radial basic non-vortical laminar flow and radial vortex flow components, respectively.

References

1. Oh JK, Park S-J, Nagueh SF: **Established and Novel Clinical Applications of Diastolic Function Assessment by Echocardiography**. *Circulation: Cardiovascular Imaging* 2011, **4**(4):444-455.
2. Buonocore MH: **Visualizing blood flow patterns using streamlines, arrows, and particle paths**. *Magn Reson Med* 1998, **40**(2):210-226.

3. Mohiaddin RH, Yang GZ, Kilner PJ: **Visualization of flow by vector analysis of multidirectional cine MR velocity mapping**. *J Comput Assist Tomogr* 1994, **18**(3):383-392.
4. Kilner PJ, Yang G-Z, Wilkes AJ, Mohiaddin RH, Firmin DN, Yacoub MH: **Asymmetric redirection of flow through the heart**. *Nature* 2000, **404**(6779):759-761.
5. Panerai RB, Smaill BH, Borst C, Chamberlain JH, Sayers BM: **A model of left ventricular function in the denervated heart**. *Journal of biomedical engineering* 1979, **1**(3):161-171.
6. Subbaraj K, Ghista DN, Fallen EL: **Intrinsic indices of the left ventricle as a blood pump in normal and infarcted left ventricles**. *J Biomed Eng* 1987, **9**(3):206-215.
7. Chahboune B, Crolet JM: **Numerical simulation of the blood-wall interaction in the human left ventricle**. *The European Physical Journal - Applied Physics* 1998, **2**(03):291-297.
8. Redaelli A, Montevecchi FM: **Intraventricular pressure drop and aortic blood acceleration as indices of cardiac inotropy: a comparison with the first derivative of aortic pressure based on computer fluid dynamics**. *Med Eng Phys* 1998, **20**(4):231-241.
9. Watanabe H, Sugiura S, Kafuku H, Hisada T: **Multiphysics simulation of left ventricular filling dynamics using fluid-structure interaction finite element method**. *Biophysical journal* 2004, **87**(3):2074-2085.
10. Merrifield R: **Patient specific modelling of left ventricular morphology and flow using magnetic resonance imaging and computational fluid dynamics**. University of Londond; 2003.
11. Long Q, Merrifield R, Xu XY, Kilner P, Firmin DN, G-Z Y: **Subject-specific computational simulation of left ventricular flow based on magnetic resonance imaging**. *Proc Inst Mech Eng H* 2008, **222**(4):475-485.
12. Kim HB, Hertzberg JR, Shandas R: **Echo PIV for flow field measurements in vivo**. *Biomed Sci Instrum* 2004, **40**:357-363.
13. Hong G-R, Pedrizzetti G, Tonti G, Li P, Wei Z, Kim JK, Baweja A, Liu S, Chung N, Houle H *et al*: **Characterization and Quantification of Vortex Flow in the Human Left Ventricle by Contrast Echocardiography Using Vector Particle Image Velocimetry**. *J Am Coll Cardiol Img* 2008, **1**(6):705-717.
14. Hong G-R, Kim M, Pedrizzetti G, Vannan MA: **Current Clinical Application of Intracardiac Flow Analysis Using Echocardiography**. *Journal of Cardiovascular Ultrasound* 2013, **21**(4):155-162.
15. Ohtsuki S, Tanaka M: **The Flow Velocity Distribution from the Doppler Information on a Plane in Three-Dimensional Flow**. *J Vis* 2006, **9**(1):69-82.
16. Uejima T, Koike A, Sawada H, Aizawa T, Ohtsuki S, Tanaka M, Furukawa T, Fraser AG: **A New Echocardiographic Method for Identifying Vortex Flow in the Left Ventricle: Numerical Validation**. *Ultrasound in medicine & biology* 2010, **36**(5):772-788.
17. Cowie MR, Wood DA, Coats AJS, Thompson SG, Poole-Wilson PA, Suresh V, Sutton GC: **Incidence and aetiology of heart failure; a population-based study**. *European Heart Journal* 1999, **20**(6):421-428.
18. Zile MR, Brutsaert DL: **New concepts in diastolic dysfunction and diastolic heart failure: Part I: diagnosis, prognosis, and measurements of diastolic function**. *Circulation* 2002, **105**(11):1387-1393.

19. Zile MR, Brutsaert DL: **New concepts in diastolic dysfunction and diastolic heart failure: Part II: causal mechanisms and treatment**. *Circulation* 2002, **105**(12):1503-1508.
20. Yu CM, Lin H, Yang H, Kong SL, Zhang Q, Lee SW: **Progression of systolic abnormalities in patients with "isolated" diastolic heart failure and diastolic dysfunction**. *Circulation* 2002, **105**(10):1195-1201.
21. Borlaug BA, Lam CS, Roger VL, Rodeheffer RJ, Redfield MM: **Contractility and ventricular systolic stiffening in hypertensive heart disease insights into the pathogenesis of heart failure with preserved ejection fraction**. *Journal of the American College of Cardiology* 2009, **54**(5):410-418.
22. Zhong L, Poh KK, Lee LC, Le TT, Tan RS: **Attenuation of stress-based ventricular contractility in patients with heart failure and normal ejection fraction**. *Ann Acad Med Singapore* 2011, **40**(4):179-187.
23. Borlaug BA, Kass DA: **Ventricular-vascular interaction in heart failure**. *Heart Fail Clin* 2008, **4**(1):23-36.
24. Borlaug BA, Paulus WJ: **Heart failure with preserved ejection fraction: pathophysiology, diagnosis, and treatment**. *European Heart Journal* 2011, **32**(6):670-679.
25. Paulus WJ, Tschope C, Sanderson JE, Rusconi C, Flachskampf FA, Rademakers FE, Marino P, Smiseth OA, De Keulenaer G, Leite-Moreira AF *et al*: **How to diagnose diastolic heart failure: a consensus statement on the diagnosis of heart failure with normal left ventricular ejection fraction by the Heart Failure and Echocardiography Associations of the European Society of Cardiology**. *European Heart Journal* 2007, **28**(20):2539-2550.
26. Paulus WJ, van Ballegoij JJM: **Treatment of Heart Failure With Normal Ejection Fraction: An Inconvenient Truth!** *J Am Coll Cardiol* 2010, **55**(6):526-537.
27. van Heerebeek L, Borbely A, Niessen HW, Bronzwaer JG, van der Velden J, Stienen GJ, Linke WA, Laarman GJ, Paulus WJ: **Myocardial structure and function differ in systolic and diastolic heart failure**. *Circulation* 2006, **113**(16):1966-1973.
28. Le T-T, Tan R-S, Huang F, Zhong L, Idapalapati S, Ghista D: **Intra-Left Ventricular Flow Distributions in Diastolic and Systolic Phases, Based On Echo Velocity Flow Mapping of Normal Subjects and Heart Failure Patients, to Characterize Left Ventricular Performance Outcomes of Heart Failure**. *Journal of Mechanics in Medicine and Biology* 2012, **12**(5).
29. Vasan RS, Larson MG, Benjamin EJ, Evans JC, Reiss CK, Levy D: **Congestive heart failure in subjects with normal versus reduced left ventricular ejection fraction: Prevalence and mortality in a population-based cohort**. *J Am Coll Cardiol* 1999, **33**(7):1948-1955.
30. Sanderson JE: **Heart failure with a normal ejection fraction**. *Heart* 2007, **93**(2):155-158.